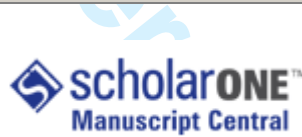




Transient and Steady State Models for Open-Loop Air-Based BIPV/T Systems

Journal:	<i>American Society of Heating, Refrigerating and Air-Conditioning Engineers, Inc.</i>
Manuscript ID:	TRNS-00088-2009.R1
Publication:	Transactions Paper
Keywords:	Residential Buildings, Solar Equipment, Building Envelope, Energy Recovery



1
2
3 Response to Reviewers Comments:
4
5
6

7 **Comment 1)**
8
9
10 I assume the omission of the film coefficient behind the back insulation container was
11 deliberate due to the order of magnitude difference in the thermal resistance between the
12 insulation and film coefficient (Figure 4).
13
14

15 **Answer:**
16
17

18 In page 9, an explanation has been included.
19
20

21 “The thermal resistance associated with the film coefficient under the insulation and
22 plywood has been neglected due to its low value compared to the thermal resistance of
23 the insulation.”
24

25 **Comment 2)**
26
27

28 It appears there are two Figure 8s. The reference on page 18 to Figure 7 applies to the first
29 Figure 8. The reference to Figure 8 on page 19 refers to the second Figure 8.
30
31

32 **Answer:**
33 The mistakes have been taken care of.
34
35

36 **Comment 3)**
37 Per policy, figure count cannot exceed 12 figures. Please reduce the number of figures
38 that appear in your document and resubmit.
39
40

41 **Answer:**
42 The numbering of figures as well as their references in the text, and the maximum
43 amount of figures has been fixed. There are only 12 figures.
44
45
46
47
48
49
50
51
52
53
54
55
56
57
58
59
60

Transient and Steady State Models for Open-Loop Air-Based BIPV/T Systems

ABSTRACT

Open-loop building-integrated photovoltaic/thermal (BIPV/T) systems with air as the heat transfer fluid can supply a substantial portion of the space heating and hot water needs of residential and commercial buildings in cold climates. Over the last few years, several customized mathematical models for these systems have been developed. This paper presents a more general model useful for design or control purposes which allows for steady-state or transient analysis. Steady state models provide a quick evaluation of the energy balance and system performance useful for design. Transient models provide more insight valuable for development of control algorithms and system design optimization.

INTRODUCTION

In building-integrated photovoltaic (BIPV) systems, photovoltaic modules are installed as functional components of the building envelope (typically, replacing cladding on facades or shingles on roofs). Since high temperatures are detrimental to the performance of photovoltaic arrays, the circulation of a cooling fluid can be used to remove thermal energy from BIPV systems. The fluid can be used for space heating or domestic hot water heating, and in the case of open loop air systems the heated air can also be used as fresh air for ventilation or for drying clothes. The integrated system is called “building integrated photovoltaic/thermal” (BIPV/T). These systems have several advantages. First, the multiplicity of functions significantly reduces costs. Second, the electrical efficiency of the photovoltaic modules is considerably improved. Finally, the proximity to the loads reduces electrical and thermal transmission losses. Properly designed BIPV/T systems may even play an aesthetic role, since they can be used to cover entire roofs, thus allowing seamless integration.

In open loop air systems, outdoor air passes through a channel under the outermost layer of the BIPV/T system which is typically the PV module or metal-roof with directly attached PV laminates (see Fig. 1 for example). Although water or glycol systems have the advantage of a much higher specific heat, air-based systems have reduced risks such as no possibility of freezing or damages to the roof due to leaks. Also, less maintenance is required and will last as long as the PV system operates (20-50 years).

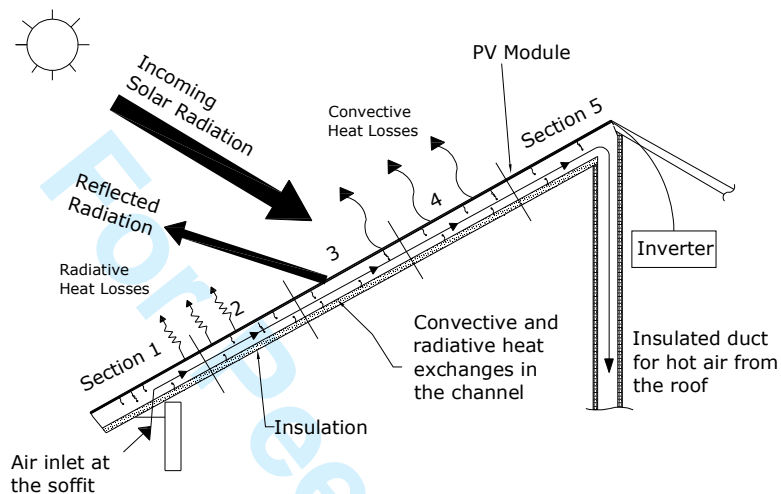
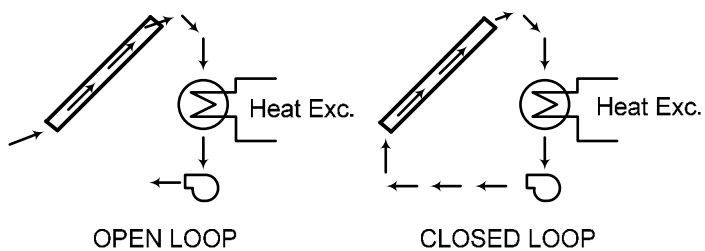


Figure 1. Schematic of a typical air-based open-loop BIPV/T system (Athienitis, 2008).

Air-based BIPV/T systems are usually installed in an open-loop configuration (see Figure 2), in which outdoor air is used to cool the PV modules by convection (commonly forced convection). The heated air is used to provide thermal energy to one or more functions in the building before being exhausted to the exterior. Open-loop air systems are normally preferred over closed loop air systems as the latter would likely lead to overheating of the PV (reducing its durability and possibly causing delamination) unless fins are built into the PV design. Also, open-loop systems allow for the potential use for fresh air preheating. Since the inlet temperatures are lower than in the case of closed-loop systems, the BIPV/T system normally operates with higher thermal efficiencies, although its air exit temperatures are lower.



1
2
3 *Figure 2. Open and closed loop configurations for solar collectors (the heat exchanger may be eliminated*
4 *in the open loop configuration).*

5
6 BIPV/T systems contain several features that complicate their study, such as heating asymmetry and a
7 relatively complex geometry. Mathematical models of different levels of complexity, emphasizing different
8 phenomena, have been developed over the years (a brief literature review is presented below). This paper
9 presents a model bringing together some of the ideas presented in previous works by the authors, and the
10 most relevant findings obtained from measurements at the experimental facilities and demonstration
11 projects of the Canadian Solar Buildings Research Network (Athienitis, 2008). This model could readily
12 be adapted as a design tool for air-based open-loop BIPV/T systems in cold climates. By incorporating
13 meteorological data, this model can be used as a decision-making tool in pre-feasibility studies.

14
15 **LITERATURE REVIEW**

16
17 **Existing Numerical Models**

18
19 Mathematical models for the particular case of forced-convection open-loop BIPV/T systems have
20 been developed by Clarke *et al.* (1997), Eicker and Fux (2000), Bazilian *et al.* (2001), Bazilian and Prasad
21 (2002), Eicker (2003) and Bloem (2004). However, many other models exist that correspond to similar
22 configurations:

- 23
24 • **Models for air hybrid photovoltaic/thermal (PV/T) collectors** – not necessarily installed as a
25 building component – have been developed by several researchers. Examples include the work of
26 Sopian *et al.* (1996) (thermal model for single and double pass hybrid PV/T air collector); Garg
27 and Adhikari (1997) (hybrid solar air collectors); and Hegazy (2000) (four configurations of
28 hybrid PV/T systems).
- 29
30 • **Models of naturally ventilated BIPV systems.** Moshfegh & Sandberg (1996) have carried out
31 CFD simulations of naturally ventilated PV façades with heating on one side to simulate solar
32 radiation. Yang *et al.* (1996) developed a numerical model for a natural ventilated PV roof and
33 façade system. The model of Brinkworth *et al.* (2000) for a natural ventilated PV in a roof
34 included a comparison with experimental results. A model of a PV/T air façade was developed in
35

1
2
3 TRNSYS and presented by Bosanac *et al.* (2003). Mittelman *et al.* (2009) developed a natural
4
5 ventilated model where Nusselt numbers are also reported.
6
7

- 8 • **Solar air heaters.** Ong (1995) developed a mathematical model and solution procedure for this
9 configuration. Ito *et al.* (2006) worked on a transient model for a glazed solar air heater.
10
11

12 At Concordia University, different BIPV/T numerical models have been developed both for research
13 on these systems and as design tools for demonstration projects. These models include the works by
14 Charron (2004), Charron and Athienitis (2006a; 2006b), Athienitis *et al.* (2005), Liao (2005), Liao *et al.*
15 (2007), Pantic (2007), Candanedo *et al.* (2007), Chen et al. (2007b) and Candanedo *et al.* (2009).
16
17

18 The aforementioned models, based on energy balances in control volumes, have used different levels
19 of complexity to model the energy interactions between the surfaces. Some of the most relevant differences
20 in approach are presented below:
21
22

23 **Common Modelling Approaches**
24
25

- 26 • **Steady state vs transient solution.** The vast majority of the models have relied on a steady state
27 approach, neglecting the thermal capacitance effects of the PV module. In contrast, Ito *et al.*
28 (2006) developed a fully-explicit finite difference model for a solar air collector. The authors
29 found that the transient model is useful to account for the effects of rapid changes (e.g., variable
30 cloudiness, wind speed fluctuations), and therefore it can be useful for the development of robust
31 control algorithms for control of flow rate.
32
33 • **Air temperature variation within the control volume.** The simplest approach uses a linear
34 approximation to model the air temperature variation within the CV (Ong, 1995). In this case, the
35 average air temperature inside the control volume is the arithmetic mean of the inlet and outlet
36 temperatures. However, most recent investigations use an exponential air temperature variation,
37 which is the exact solution if the temperatures of the surrounding surfaces are assumed to be
38 uniform inside the CV. The average air temperature (used for the energy balances) is calculated as
39
40

41
42
43
44
45
46
47
48
49
50
51
52
53 $T_{avg} = \frac{\int T dx}{\Delta x}$.
54
55
56
57
58
59
60

- 1
2
3 • **Radiative heat transfer.** Most investigations have used the mean temperature of the surrounding
4 surfaces (T_m) to calculate a linearization factor ($\frac{4\sigma T_m^3}{\varepsilon_1 + \varepsilon_2 - 1}$), as this facilitates the solution of the
5
6

7 equations. The radiatiave heat transfer coefficient, h_r is given then by
$$\frac{4\sigma T_m^3}{\left(\frac{1}{\varepsilon_1} + \frac{1}{\varepsilon_2} - 1\right)}$$
,
8
9

10 assuming a view factor of 1 between the plates. The radiation exchange difference by using this
11 coefficient assuming two plates at 350 and 273 K is about 1.5% underestimated from the exact
12
13

14 value given by the equation
$$\frac{\sigma(T_2^4 - T_1^4)}{\left(\frac{1}{\varepsilon_1} + \frac{1}{\varepsilon_2} - 1\right)}$$
.

- 15
16
17
18
19
20 • **Effect of view factors.** The majority of the models assume, often without stating it explicitly, that
21 the view factor between the two surfaces of interest is close to 1. In reality, this assumption is not
22 always accurate. Charron (2004) took view factor calculations for radiative heat transfer modelling
23 into account.
24
25
26
27
28 • **Convective interior heat transfer correlations.** As explained above, heat transfer in BIPV/T has
29 several particularities due to the assymetric heating (i.e., heat transfer occurs mainly through one
30 side of the BIPV/T channel) and the more complex geometry. However, most researchers have
31 used Nusselt number correlations developed for pipes and ducts with uniform boundary conditions
32 for a given cross section, such as the classic correlation by Dittus and Boelter (1930), and the
33 Pethukov equation (Bazilian *et al.*, 2001; Eicker, 2003). These correlations tend to underestimate
34 convective heat transfer coefficients, because several heat-transfer enhancing factors are not taken
35 into account, such as the presence of the framing structure and surface imperfections (which act as
36 turbulence promoters) and developing flow conditions at the inlet.
37
38
39
40
41
42
43
44
45
46 • **Convective and radiative exterior heat transfer coefficients.** The determination of the heat loss
47 to the surroundings has been carried out through many different approaches. The McAdams
48 formula reported by Duffie & Beckman (2006) developed in the 50s, combines radiation and
49 convection into one coefficient. The McAdams formula has often been used (Ong, 1995; Ito *et al.*,
50 2006). This approach is satisfactory for glazed collectors, since the addition of the glass layer
51 significantly increases the insulation, and the effect of the exterior heat transfer coefficients
52 becomes less important. Most researchers separate exterior heat losses in two components:
53
54
55
56
57
58
59
60

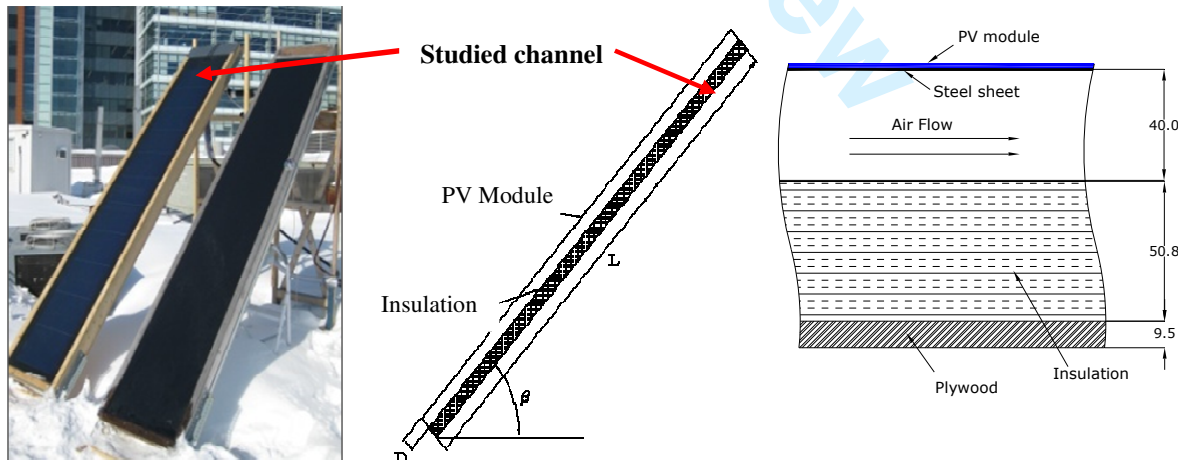
convection to the exterior air and radiation to a representative sky temperature. The convective heat transfer correlations by Test (1981) and Sharples & Charlesworth (1998) were developed for roof-mounted flat-plate collector and are preferable to the McAdams formula, as confirmed by the experimental observations mentioned in this paper. Both correlations have been used in modelling BIPV/T systems (Chen, 2009). The Model by Berdahl & Martin (1984) presented a simplified calculation for a representative sky temperature, which can be used to calculate radiative heat transfer losses.

- **Incidence angle adjustments.** Few researchers have accounted for the effect of the variation of the optical properties (transmittance, reflectance, absorptance) of the significant surfaces as a function of the angle of incidence. In contrast, incidence angle adjustments has often been considered in investigations dealing with the electrical performance of PV and BIPV systems (Fanney *et al.*, 2003; King *et al.*, 2004).
- **Effect of moisture content.** Moisture has an important effect on the physical characteristics of the fluid, in particular on the effective specific heat of the air, accounting for a 1-4% increase with respect to the specific heat of dry air. This effect is less significant under cold winter conditions.
- **Inlet air temperature effects.** In BIPV/T systems, the inlet air temperature is sometimes slightly higher than the exterior air temperature. This is especially true in BIPV/T roofs, where the inlet air has been warmed by thermal energy released by the building's façade. However, few works have considered this effect in BIPV/T modeling (Saelens *et al.*, 2004).
- **Electrical efficiency modeling.** Most BIPV/T investigations account for the effect of the PV modules' temperature on their electrical efficiency with a very simple linear model (Candanedo *et al.*, 2007).
- **Equations solving method.** A common approach has been to linearize all the equations and solve the resulting linear system by matrix inversion. Since the system of equations is relatively robust, it can be solved by the simple method of assuming guess values and iterating until a convergence criterion is met. When the effects of thermal inertia are considered, a transient method, such as the fully explicit finite difference method has been used.

- 1
2
3 • **Pressure drop.** The modeling of the pressure drop in the air channel has been largely overlooked
4 in most previous work. It is worth mentioning, however, that the measured pressure drops along
5 BIPV/T roofs and façades is often much smaller than the pressure drop along the ducting system.
6
7 Pressure drop is evidently a strong function of the geometric configuration of the channel,
8 especially of the framing system used to support the BIPV/T. Since the modules repeat themselves
9 at regular intervals, the air pressure follows a “spatially periodic” variation inside the BIPV/T
10 channel, with an overall linear trend.
11
12
13
14
15

EXPERIMENTAL FACILITY

18
19
20 The models developed are mainly based on experimental data obtained in a test channel located at
21 Concordia University, which is shown in Figure 3. The BIPV/T channel was built to simulate a section of
22 the roof at the EcoTerra demonstration house (Chen *et al.*, 2007a). It is shorter in length however due to
23 practical construction limitations. The top of the channel consists of an amorphous PV module, with a 6%
24 efficiency under standard test conditions, glued to a 0.02 in. (0.5 mm) stainless steel sheet. The bottom of
25 the channel consists of 2 inches of polystyrene insulation R-10 (1.76 Km²/W) and 3/8 in. thick plywood
26 board (see Figure 3). There is a 1.57 in (0.04 m) gap between the PV module and the board (D). A wooden
27 frame keeps the top and bottom parts together. The channel's length (L) in the flow direction is 112 in.
28 (2.84 m), and its width is 15.23 in. (0.387 m). The channel is oriented with a due-south azimuth angle and a
29
30 tilt angle (β) of 45°.
31
32
33
34
35
36
37
38
39



55 Figure 3. Experimental set-up used for model development. From left to right: photograph of the
56 BIPV/T channel, simplified side view and details of the channel configuration (dimensions in mm).
57
58
59
60

The visible reflectance of the PV module surface has been measured with a reflectometer as 4.3% at a normal incidence angle and it would be expected that the solar value would be close to the visible one. The longwave emissivity of the amorphous PV panel has been taken as 0.95 (LESO-PB/EPFL *et al.*, 2000). The measured emissivity of the steel plate is 0.80 while the corresponding value for the insulation board is 0.20. Thermocouples are installed at the interior surface of the PV module and on the insulation (i.e., top and bottom of the channel) at nine different positions along the channel. Other measured variables include the electrical output of the PV module, solar irradiation, wind speed and relative humidity. No thermocouples were installed on top of the PV module, as the resulting shading would have reduced the electrical output.

The air flow rate was controlled in the experiments; it was measured with a laminar flow element, with an accuracy of 0.4% of the full-scale (105 CFM). The maximum achievable flow rate in the channel is 50 CFM (23.6 L/s), corresponding to an average air velocity in the channel of 5 ft/s (1.55 m/s).

The amorphous PV module is constructed from different layers. These are from top to bottom, Tefzel, antireflectice coating, amorphous silicon, a backing substrate, tefzel, adhesive and a stainless steel layer to where it was pasted. The Models used the material properties summarized in Table 1.

TABLE 1
Material Parameters

Layer	Parameter	Value IP (SI)
TEFZEL	Thickness	0.039 in. (1 mm)
TEFZEL	Density	109.2 lb _m /ft ³ (1750 kg/m ³)
TEFZEL	Specific Heat	0.251 Btu/lb _m °F (1050 J/kg·K)
TEFZEL	Thermal conductivity	0.139 Btu/h·ft°F (0.24W/m·K)
Anti reflective coating	Thickness	1.9E ⁻⁵ in. (5E ⁻⁴ mm)
Silicon	Thickness	1.9E ⁻⁵ in. (5E ⁻⁴ mm)
Silicon	Density	145.4 lbm/ft ³ (2330 kg/m ³)
Silicon	Thermal conductivity	85.5 Btu/h·ft°F (148 W/m·K)
Backing substrate (steel)	Thickness	7.87E ⁻³ in. (0.2 mm)
Backing substrate (steel)	Density	493.181 lb _m /ft ³ (7900 kg/m ³)
Backing substrate (steel)	Specific Heat	0.114 Btu/lb _m °F(477 J/kg·K)
Backing substrate (steel)	Thermal conductivity	8.61 Btu/h·ft°F (14.9 W/m·K)
TEFZEL	Thickness	0.039 in. (1mm)
Adhesive (Ethylene propylene copolymer)	Thickness	0.024 in. (0.6 mm)
Adhesive (Ethylene propylene copolymer)	Density	134.22 lb _m /ft ³ (2150 kg/m ³)
Adhesive (Ethylene propylene copolymer)	Specific Heat	0.263 Btu/lb _m °F (1100 J/Kg·K)
Adhesive (Ethylene propylene copolymer)	Thermal Conductivity	0.116 Btu/h·ft°F (0.2 W/m·K)
Steel sheet	Thickness	0.02 in. (0.5 mm)

PROPOSED MODELS: STEADY STATE AND TRANSIENT

Assumptions

- The temperatures of the surfaces (PV, steel sheet, insulation board) are assumed to be uniform inside the control volume.
- The resistance of the PV module is taken into account in the calculations.
- No temperature variations are considered across the width of the channel (1-D simulation inside the control volume).
- No edge effects are considered.
- Properties of solid materials remain constant and uniform.
- No air leakage or mixing with exterior air after entering the air gap.
- No humidification or dehumidification of the air stream.
- Convective heat transfer is higher at the entrance region before fully developed conditions are established. However, since the focus of this study is the final air temperature and the average PV module temperature, a single uniform value was used for the interior convective heat transfer coefficients (h_{ct} , h_{ch}) for a given air speed.

Models Considered

The two models considered here are shown schematically in Figure 4. The thermal resistance associated with the film coefficient under the insulation and plywood has been neglected due to its low value compared to the thermal resistance of the insulation. The two models are identical except in one respect: steady state model does not consider the thermal capacitance of the PV panel (making it a steady-state model), while transient model takes into account the thermal inertia (capacitance) of the PV panels. In a dynamic simulation, the solution of the equations of the steady state model is independent of previous conditions. In contrast, at every time step, the transient model requires the solution of the previous time step with a fully-explicit finite difference scheme. The programming tool MATLAB® is used to numerically find the solution of both models.

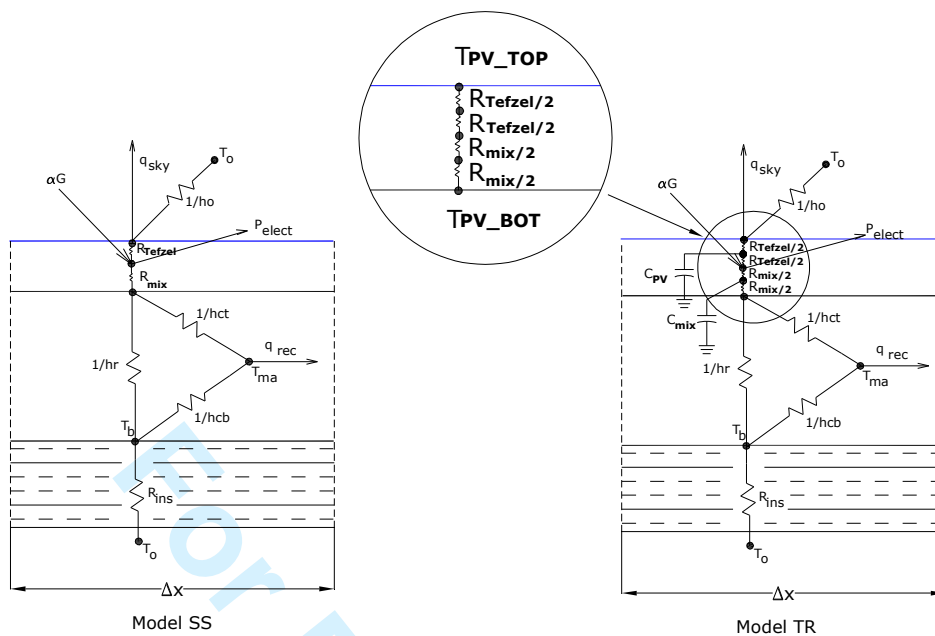


Figure 4. Models studied: Model SS (steady state) and Model TR (transient).

Steady State (SS) Model

The equations corresponding to a representative control volume in Model SS are shown below. Equations 1 through 5 respectively correspond to energy balances at the top surface of the PV module, middle of the PV module, bottom surface of the PV module, air node and the surface of the insulation:

$$\frac{T_{PV_MID} - T_{PV_TOP}}{R_{Tefzel}} - \varepsilon_1 \sigma (T_{PV_TOP}^4 - T_{sky}^4) - (T_{PV_TOP} - T_o) h_o = 0 \quad (1)$$

$$\alpha(\theta)G - P_{elect} + \frac{(T_{PV_MID} - T_{PV_TOP})}{R_{Tefzel}} + \frac{(T_{PV_MID} - T_{PV_BOT})}{R_{Mix}} = 0 \quad (2)$$

$$\frac{(T_{PV_MID} - T_{PV_TOP})}{R_{Mix}} - q_{rad} - (T_{PV_BOT} - T_{ma}) h_{ct} = 0 \quad (3)$$

$$(T_{PV_BOT} - T_{ma}) h_{ct} + (T_b - T_{ma}) h_{cb} = q_{rec} \quad (4)$$

$$q_{rad} + (T_b - T_{ma})h_{cb} + \frac{T_b - T_o}{R_{ins}} = 0 \quad (5)$$

$$q_{rad} = \sigma F_{PV,b} \left(\frac{1}{\varepsilon_2} + \frac{1}{\varepsilon_3} - 1 \right)^{-1} \left(T_{PV_{BOT}}^4 - T_b^4 \right) \quad (6)$$

$$\eta_{PV} = \eta_{STC} (1 - \beta (T_{PV_{MID}} - 25^\circ C)) \quad (7)$$

$$P_{elect} = \eta_{PV} \alpha(\theta) G \quad (8)$$

$$T_{outlet} = T_{inlet} + \frac{A_{cv} q_{rec}}{\dot{m} c_p \text{air}} \quad (9)$$

$$T_{ma} = \frac{1}{\Delta x} \int_0^{\Delta x} \left(\frac{h_{ct} T_{PV_{BOT}} + h_{cb} T_b}{h_{ct} + h_{cb}} + e^{-\frac{W_{PV}(h_{ct} + h_{cb})}{\dot{m} c_p} x} \right) dx \quad (10)$$

In the equation system presented above, there are nine unknowns: $T_{PV_{TOP}}$, $T_{PV_{BOT}}$, T_b , q_{rad} , η_{PV} , P_{elect} , T_{ma} , T_{outlet} and q_{rec} . The rest of the variables (solar radiation, exterior temperature, mass flow rates, material properties, etc.) are known inputs. However, several additional equations are used:

- The view factor $F_{PV,b}$ is calculated as a function of geometric parameters (Incropera & De Witt, 2002).
- The absorptance α of the exposed PV surface is corrected as a function of the angle of incidence of beam solar radiation, as described by King *et al.* (1997). The effect of the angle of incidence is significant during the early morning hours and late afternoon hours. For these models, a correction curve developed specifically for the amorphous PV laminate, calculated according to the procedure described by King *et al.* (1997) and available at the Sandia National Laboratories database (2006), was used.

- The sky temperature employed to calculate radiative heat losses to the exterior is obtained with the following formula (Duffie & Beckman, 2006) :

$$T_{sky} = T_a \cdot (0.711 + 0.0056 \cdot T_{dp} + 0.000073 \cdot T_{dp}^2 + 0.013 \cos(\pi \cdot t / 12)) \quad (11)$$

- The specific heat of air (c_p) has been calculated for the conditions of temperature and relative humidity measured at the inlet of the channel.
- The exterior convective heat transfer correlation is obtained using different correlations to compare their effects into the results. These are the correlations by Test *et al.* (1981), Sharples & Charlesworth (1998), McAdams (Duffie & Beckman, 2006) as a function of the wind speed in m/s:

$$h_o = 8.55 + 2.56V_{wind} \quad (12)$$

$$h_o = 11.9 + 2.2V_{wind} \quad (13)$$

$$h_o = 5.7 + 3.8V_{wind} \quad (14)$$

- The interior convective heat transfer coefficients (h_{ct} and h_{cb}) have been calculated as average values for the entire channel, according to correlations developed for this case as a function of the air speed inside the channel:

$$h_{ct} = 8.38V_{ch} + 1.76 \quad (15) \qquad h_{cb} = 13.28e^{1.73V_{ch}} \quad (16)$$

The asymmetric heating conditions inside the channel cause h_{cb} to be much larger than h_{ct} , with the consequence that the average air temperature (T_{ma}) is closer to T_b than to $T_{PV,bot}$. This result has been confirmed by CFD analysis (see Figure 5) and experimental results in the channel.

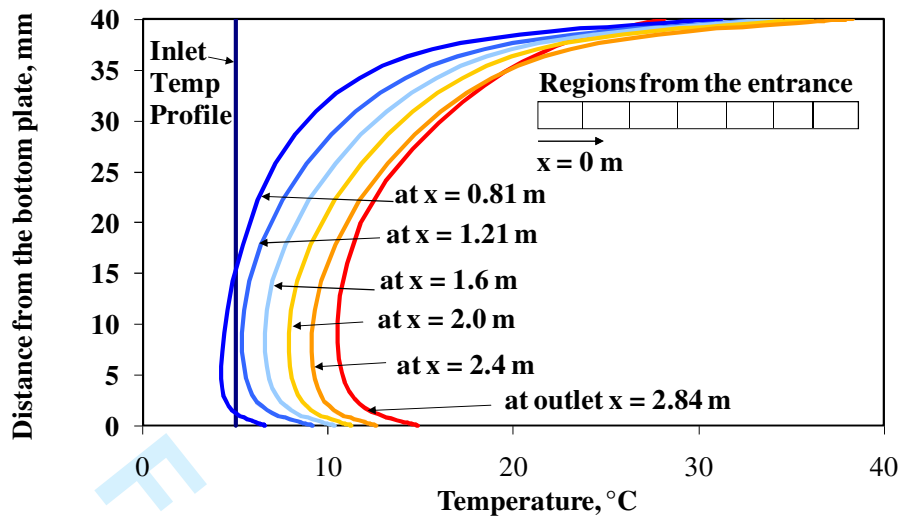


Figure 5. Air temperature profiles within the channel as predicted by CFD simulations.

It is evident from Figure 5 that the average air temperature is closer to the temperature measured at the bottom of the channel. However, the heat flux through the top of the channel is much larger than the heat transferred from the bottom of the channel to the airstream. As the insulation creates nearly adiabatic conditions, heat loss through the bottom is practically negligible.

Transient (TR) Model

As mentioned above, the transient model includes the thermal capacitance of the PV module. In this case, a fully-explicit scheme has been used (the temperatures for the current time step depend only on the temperatures of the previous time step). Equation 18 corresponds to the energy balance in a node associated with a mid-layer of the PV module. This node has a capacitance per unit area of 1800 J/Km^2 , obtained from estimates of material properties. Capacitances are included only in the top part of PV module, since it is exposed to rapidly changing weather conditions including wind and irradiance, whereas the bottom of the channel is insulated. The equations corresponding to the transient model are:

$$\frac{T_{MID1,i+1} - T_{PV_{TOP},i}}{R_{Tefzel}/2} - \varepsilon_1 \sigma \left(T_{PV_{TOP},i+1}^4 - T_{sky,i+1}^4 \right) - (T_{PV_{TOP},i+1} - T_{o,i+1}) h_o = 0 \quad (17)$$

$$T_{MID1,i+1} = T_{MID1,i} + \frac{\Delta t}{C_{PV}} \left(\frac{T_{PV_{TOP},i} - T_{MID1,i}}{R_{Tefzel}/2} + \frac{T_{PV,i} - T_{MID1,i}}{R_{Tefzel}/2} \right) \quad (18)$$

$$T_{PV_{i+1}} = \left(\frac{\frac{T_{MID1,i}}{R_{Tefzel}/2} + \frac{T_{MID2,i}}{R_{Mix}/2} + \alpha(\theta)_i G_i - P_{elect,i}}{\frac{1}{R_{Tefzel}/2} + \frac{1}{R_{Mix}/2}} \right) \quad (19)$$

$$T_{MID2,i+1} = T_{MID2,i} + \frac{\Delta t}{C_{Mix}} \left(\frac{T_{PV,i} - T_{MID2,i}}{R_{Tefzel}/2} + \frac{T_{PV_{BOT},i} - T_{MID2,i}}{R_{Tefzel}/2} \right) \quad (20)$$

$$q_{rec,i+1} = h_{ct} (T_{PV_{BOT},i} - T_{ma,i}) + h_{cb} (T_{b,i} - T_{ma,i}) \quad (21)$$

$$T_{b,i+1} = \frac{T_{ma,i} h_{cb} + \frac{T_{o,i}}{R_{ins}} + q_{rad,i}}{h_{cb} + \frac{1}{R_{ins}}} \quad (22)$$

$$q_{rad,i+1} = \sigma F_{PV,b} \left(\frac{1}{\varepsilon_2} + \frac{1}{\varepsilon_3} - 1 \right)^{-1} \left({T_{PV_{BOT},i}}^4 - {T_{b,i}}^4 \right) \quad (23)$$

$$\eta_{PV,i+1} = \eta_{STC} (1 - \beta (T_{PV,i} - 25^\circ C)) \quad (24)$$

$$P_{elect,i+1} = \eta_{PV,i} \alpha_i G_i \quad (25)$$

$$T_{outlet,i} = T_{inlet,i} + \frac{A_{CV} q_{rec,i}}{\dot{m} c_{p_air}} \quad (26)$$

$$T_{ma,i+1} = \frac{1}{\Delta x} \int_0^{\Delta x} \left(\frac{h_{ct} T_{PV_{BOT},i} + h_{cb} T_{b,i}}{h_{ct} + h_{cb}} + e^{-\frac{W_{PV}(h_{ct} + h_{cb})}{\dot{m}_i c_{p_air}} x} \right) dx \quad (27)$$

The magnitudes corresponding to the time step $i+1$ are written as a function of the magnitudes of the previous time step i . In equation 17, the solution for $T_{PV_{TOP},i+1}$ is found numerically with the MATLAB® function *fzero*, as the rest of the parameters are known as inputs or as the result of the previous time step. The corrections corresponding to incidence angle, specific heat, view factor and heat transfer coefficients were also applied for the transient model.

In both the steady state and the transient models, the channel can be divided into an arbitrary number of control volumes. The inlet conditions of a control volume correspond to the outlet conditions of the previous control volume.

RESULTS

Model Performance

The transient and steady state models were applied with input measurements (solar radiation, exterior temperature, wind speed, and channel flow rate) corresponding to February 17th, 2009. During this day, the flow rate in the channel was changed manually several times. Figure 6a shows the measured average air speed inside the channel, and the estimated interior heat transfer coefficients according to equations 12 and 13. The wind speed was measured during this interval as well. The correlations by Test (Equation 11) Sharples & Charlesworth and McAdams were used to estimate the exterior heat transfer coefficient (Figure 6b).

In both the steady state and the transient models, four control volumes were used. Results corresponding to the average temperature of the top of the channel (Figure 6a) and the outlet temperature of the air (Figure 6b) are presented. The time step used for the transient model was 1 second. The output of both models is compared to thermocouple measurements taken at intervals of 1 minute. Exterior air temperature and solar radiation measurements are presented as well. In general, there is a reasonably good agreement between both models and the experimental results. Perhaps the most relevant difference between the models is that the temperature fluctuations predicted by the transient model are much smaller than those predicted by the steady state model. In this respect, the transient model (which includes the capacitive effect) is more accurate than the steady state model. The presence of the capacitance considerably stabilizes the temperatures in the PV module, and dramatically reduces the effect of the varying wind speed (and its associated heat transfer coefficient) and solar radiation changes.

The effect of the exterior convective correlation on the average temperature of the top of the channel can be observed in Figure 7. In general, the McAdams correlation overpredicts the temperature of the top of the channel. Test and Sharples' correlations give better estimations to the average PV bottom surface

temperature. Although the Sharples correlation give better results, for high wind velocities it seems to overestimate the h_o value.

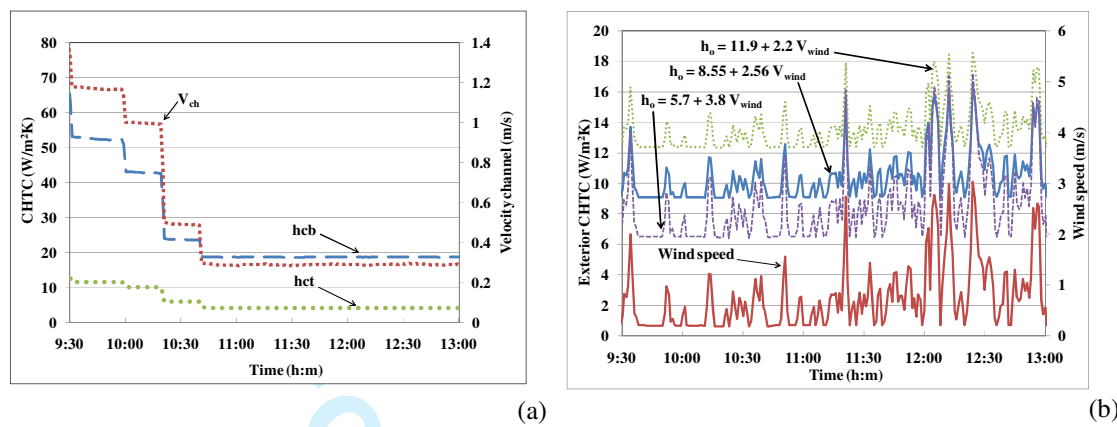


Figure 6. (a) Measured average air speed in the channel, and estimated interior heat transfer coefficients; (b) Wind speed and exterior heat transfer coefficient.

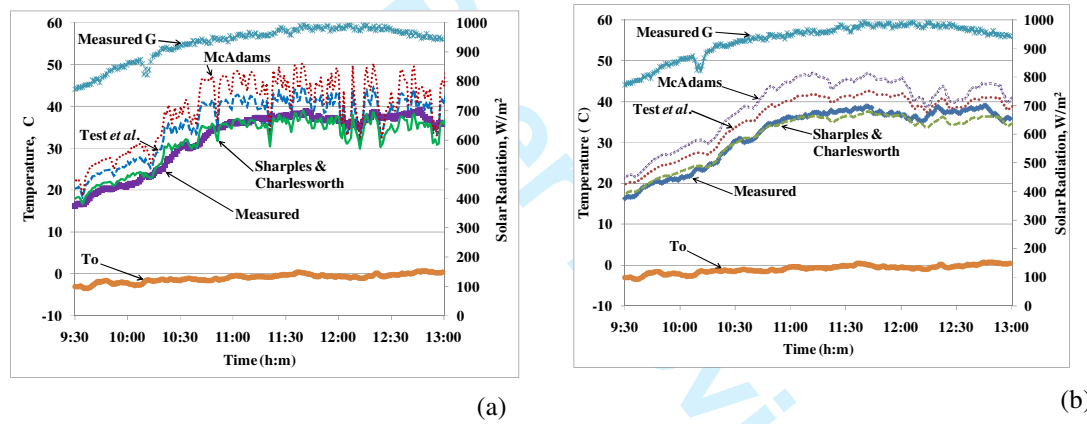


Figure 7. (a) Average temperature of the top of the BIPV/T channel (measurements, Model SS), (b) Average temperature of the top of the BIPV/T channel (measurements, Model TR) Solar radiation incident on collector (G) and exterior air temperatures (T_o) are also shown.

The predicted outlet air temperature obtained with Sharples & Charlesworth correlation with the SS and TR models is plotted in figure 8. The agreement with the experimental data was good in general.

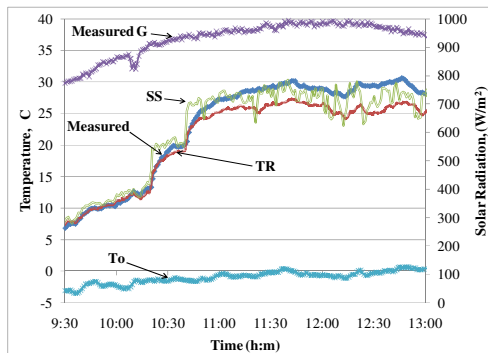


Figure 8. Outlet air temperatures (measurements, Model SS and Model TR)

The transient model with Test correlation practically mirrors the measured curve with an offset of a few degrees, which becomes very small between 12:00 and 13:00. Interestingly, this is the time when the highest wind speed values were recorded (about 1.5 m/s, versus 0.5 m/s earlier in the day). This result suggests that the test correlation under-predicts \dot{m} at low wind speeds. This can be attributed to local natural convection effects (not considered in most correlations) that may become the dominant factor at low wind speeds.

Most researchers have neglected the resistance of the PV module, implicitly assuming that the temperature of the top and bottom faces of the PV are the same. However, recent investigations have included the resistance of the PV module (Ji *et al.*, 2009). Even if the PV resistance is very small, the heat flux across the PV module represents a difference of a couple of degrees between both sides. For example, if a heat flux of 300 W/m² passes through a PV module having a resistance of 0.01 Km²/W, the temperature difference between both sides is 3 °C. This resistance is not negligible, since there are several layers of material (steel substrate, encapsulation, vinyl, adhesive, etc.).

Demonstration Project: Ecoterra House

The transient model was applied to data recorded at the EcoTerra™ demonstration house BIPV/T system (Xiang et al. 2007). This was a prefabricated modular house, with the BIPV/T system built as one of the modules in the factory. This is the first time such a BIPV/T system is constructed in a factory. Photographs of the BIPV/T module of the house and of the completed house are shown in Figures 9 and 10. Among the input parameters used in the model are: ambient air temperature, inlet air temperature, insulation R-value, total solar radiation incident on the plane of the PV modules and flow rates. The wind speed was not being recorded for this specific day. The wind speed employed was the one of the neighboring city of Sherbrooke. The results are summarized in Figure 11. The length of the roof (flow path) is 5.8 m and the air cavity thickness is 0.038 m.



Figure 9. Left: BIPV/T module of the roof under construction in the factory (before installing metal layer and PV modules) Right: BIPV/T module completed (with PV modules installed).



Figure 10. EcoTerra™ solar house photograph

Good agreement was observed between the measured data for the PV back surface temperature and the transient simulation result. There was good agreement for the T_b temperature. For the outlet air temperature, the agreement was acceptable but not as good as for TPV and T_b . The temperature difference between 10:40 and 11:20 a.m. is probably due to the thermal capacitance of the wood framing, which is not modeled, and error in the measurement of the flow rate across the BIPV/T roof.

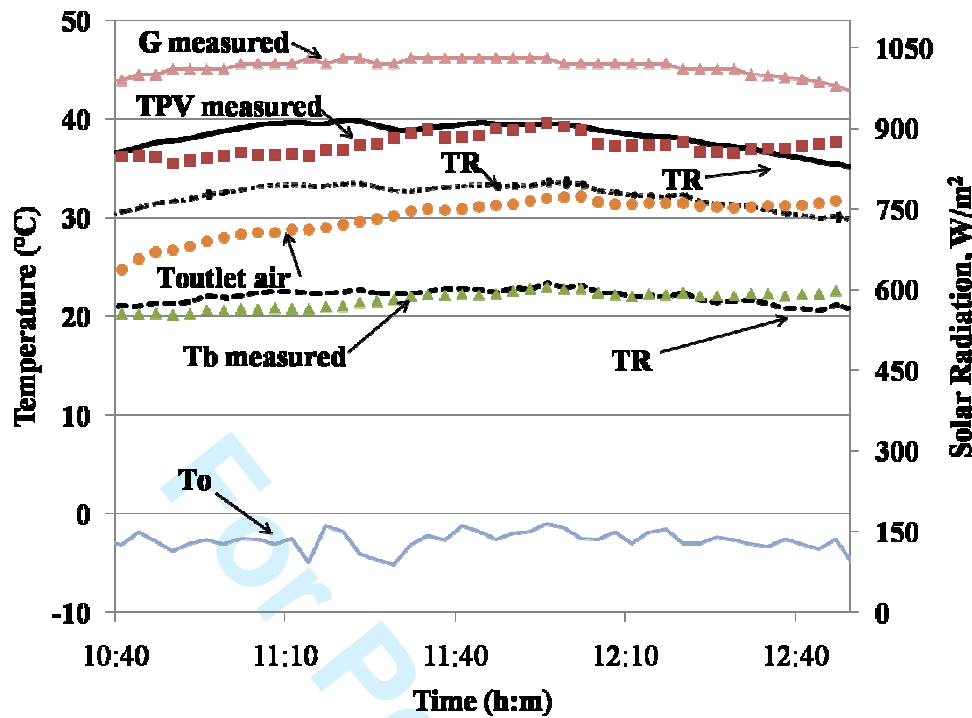


Figure 11. Temperature profiles for the EcoTerra house on March 17th, 2008 (measurement and Model TR)

Heat Removal Factor and Thermal Efficiency

If the BIPV/T channel is treated as a solar collector, a modified form of the Hottel-Whillier-Bliss equation which includes the electricity output can be written as:

$$Q_u = F_R A_c (\alpha G - P_{elect} - U_L (T_i - T_a)) \quad (28)$$

In this case, U_L represents the heat loss coefficient (W/m^2) from the air in the BIPV/T channel to the ambient air. Neglecting the heat loss through the bottom of the BIPV/T channel, we can write:

$$U_L = ((h_o + h_r)^{-1} + R_{PV})^{-1} \quad (29)$$

Ordinary solar collectors are often designed with a glazing cover and an absorber plate to prevent heat losses, and their U_L depends mainly on geometric parameters and the materials used, and the influence of convective and radiative coefficients is small. In contrast, in this BIPV/T channel, U_L undergoes significant

changes with the convective and radiative coefficients. The heat removal factor (F_R) can be determined experimentally by solving for it in Equation 28.

$$F_R = \frac{Q_U}{A_c(\alpha G - P_{elect} - U_L(T_i - T_a))} \quad (30)$$

By dividing Equation 28 by the solar radiation times the area (GA_c), and using the fact that $P_{elect} = \eta_{PV}G$, the following expression for thermal efficiency is obtained:

$$\eta_{Th} = F_R \left(\alpha - \eta_{PV} - U_L \frac{T_i - T_a}{G} \right) \quad (31)$$

As expected, this equation implies that the maximum thermal efficiency occurs when the inlet temperature is equal to the ambient temperature, which makes an open-loop configuration desirable. The thermal efficiency is always smaller than the heat removal factor. Figure 12 shows the heat removal factor calculated with Equation 25 (assuming that the R_{PV} value is 0.01 RSI) for February 17th, 2009, and the

thermal efficiency calculated simply as $\eta_{Th} = \frac{mc_p \Delta T}{GA_c}$. As expected, the efficiency is higher when the flow rates inside the

channel are higher.

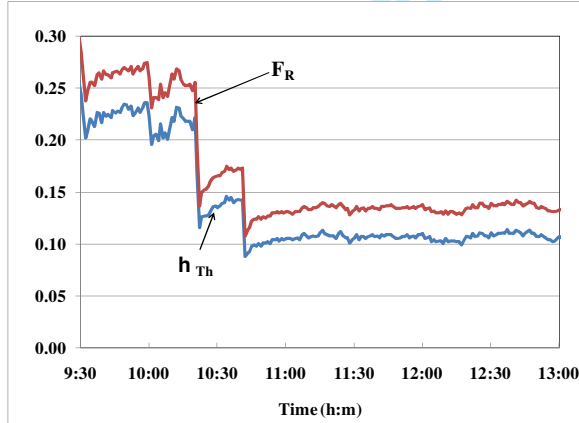


Figure 12. Heat removal factor and thermal efficiency of the BIPV/T channel.

The pressure drop measurements for this channel are relatively small; for a flow rate of 50 CFM (23.6 L/s), the pressure drop is less than 9 Pa. Assuming that the combined efficiency of the electric motor and the fan is only 20%, the resulting electric power consumption would be: $(0.0236 \text{ m}^3/\text{s})(9 \text{ Pa})/0.20 = 1.06$

W. This result illustrates the usefulness of air-based BIPV/T systems, as the required power consumption for driving the flow in the channel is small in comparison with the recovered energy (in this case, 68 W of electric power, and hundreds of Watts of thermal energy). Pressure drop along the channel is likely to be even smaller if the cross section area is larger. This information is very useful for design purposes: it suggests that it is advisable to minimize the ducting system, since the most significant pressure drops will be much larger there than in the BIPV/T channel. As expected, for higher flow rates the efficiency is much higher (e.g. during the time period 9:30 -10:30am in Fig. 10) due to the higher heat transfer coefficients.

CONCLUSIONS

In this paper, two models for air-based open-loop BIPV/T systems have been presented. The models included phenomena that have often been neglected, including the effect of the solar incidence angle, resistance and capacitance of the PV module, view factors between plates and the variation of specific heat with moisture content.

In general, the transient model, which includes thermal capacity effects of the PV, follows experimental measurements better than the steady state model. The transient model indicates as well a more stable outlet air temperature which reflects the damping effect of the heat capacitance of the materials. However, the transient model is probably not necessary for system design as it does not significantly improve average accuracy and requires more processing time and more inputs. The transient model is suitable for development of optimal control algorithms of the air flow rate.

The model performance could be improved by: (a) using a more accurate correlation for the exterior heat transfer coefficient, and (b) using values for resistance and capacitance of the PV module that are either provided by the manufacturer or experimentally measured. Detailed correlations for the cavity heat transfer coefficient are under development.

ACKNOWLEDGEMENTS

This work was funded by the Canadian Solar Buildings Research Network, a strategic NSERC research network and NRCan-CanmetENERGY (Varennes); we would also like to acknowledge the technical and other support of Dr. Yves Poissant and Josef Ayoub. The technical assistance of Joseph Hrib and Kwang Wook Park in the set up of the experiment is gratefully acknowledged. The third author would

like to acknowledge the financial support of NSERC through a CGS D2 Alexander Graham Bell Graduate Scholarship.

NOMENCLATURE

A_c	Exposed area of the BIPV/T collector, m^2
A_{cv}	Area of the control volume, m^2
F_{PV}	View factor between the surfaces
C_{pv}	Thermal capacitance per unit area, $\text{J}/(\text{kg}\cdot\text{K}\cdot\text{m}^2)$
c_p	Specific heat of the air, $\text{J}/(\text{kg}\cdot\text{K})$
F_R	Heat removal factor
G	Total incident solar radiation on the plane of the collector per unit area, W/m^2
h_o	Exterior convective heat transfer coefficient or wind coefficient per unit area, $\text{W}/(\text{m}^2\text{K})$
h_r	Cavity radiative heat transfer coefficient per unit area, $\text{W}/(\text{m}^2\text{K})$
h_{ct}	Convective heat transfer coefficient for the top surface per unit area, $\text{W}/(\text{m}^2\text{K})$
h_{cb}	convective heat transfer coefficient for the bottom surface per unit area, $\text{W}/(\text{m}^2\text{K})$
i	Sub-index, time step counter
P_{elect}	Electrical power per unit area, W/m^2
T_{ma}	Average air temperature, $^\circ\text{C}$
q_{sky}	Radiative heat loss to the sky per unit area, W/m^2
q_{rec}	Heat recovered in the control volume per unit area, W/m^2
Qu	Total heat recovered in the BIPV/T collector, W
R_{PV}	Thermal resistance of the PV module, $\text{m}^2\text{K}/\text{W}$
R_{ins}	Combined thermal resistance of the insulation and plywood layer, $\text{m}^2\text{K}/\text{W}$
T_a	Ambient air temperature, $^\circ\text{C}$
T_{dp}	Dew point temperature, $^\circ\text{C}$
T_o	Ambient air temperature, $^\circ\text{C}$
$T_{PV_{TOP}}$	PV exterior surface temperature, $^\circ\text{C}$
$T_{PV_{MID}}$	PV temperature at the middle of module, $^\circ\text{C}$
$T_{PV_{BOT}}$	PV interior surface temperature, $^\circ\text{C}$
T_b	Interior insulation temperature, $^\circ\text{C}$
t	time from midnight, hr
U_L	Heat loss coefficient, $\text{W}/(\text{m}^2\text{K})$
W	Width of the control volume, m
V_{wind}	Wind speed, m/s
V_{ch}	Air speed in the channel, m/s

Greek Letters

α	Solar absorptance
β	PV module temperature coefficient ($\% \text{K}^{-1}$)
Δx	length of control volume, m
ϵ	Surface long-wave emissivity
η_{PV}	electrical efficiency of the PV module
η_{STC}	electrical efficiency at standard test conditions

Acronyms

BIPV	Building Integrated Photovoltaic
BIPV/T	Building Integrated Photovoltaic/Thermal
PV/T	Photovoltaic/Thermal
SS	Steady State
TR	Transient

θ Incidence angle, degrees

References

- Athienitis A.K., 2008, "Design of Advanced Solar Homes Aimed at Net-zero Annual Energy Consumption in Canada", ISES-AP - 3rd International Solar Energy Society Conference – Asia Pacific Region, Sidney, Australia, Nov., 14 pages
- Athienitis AK, Poissant Y, Collins M & Liao L. (2005). Experimental and numerical results for a building-integrated photovoltaics test facility. *Photovoltaic Specialists Conference, 2005 Conference Record of the Thirty-first IEEE*, 1718-1721.
- Bazilian M, Groenhout NK & Prasad D. (2001). Simplified numerical modelling and simulation of a photovoltaic heat recovery system. In *17th European photovoltaic solar energy conference*, pp. 2387-2390. Munich, Germany
- Bazilian MD & Prasad D. (2002). Modelling of a photovoltaic heat recovery system and its role in a design decision support tool for building professionals. *Renewable Energy* **27**, 57-68.
- Berdahl P & Martin M. (1984). Emissivity of clear skies. *Solar Energy* **32**, 663-664.
- Bloem JJ. (2004). A TRNSYS type calculation model for double skin photovoltaic facades. *Proc 19th European Photovoltaic Solar Energy Conference and Exhibition, Paris, France, 2004*.
- Bosanac M, Sorensen B, Katic I, Sorensen H, Nielsen B & Badran J. (2003). Photovoltaic thermal solar collectors and their potential in Denmark, pp. 1-114.
- Brinkworth BJ, Marshall RH & Ibarahim Z. (2000). A validated model of naturally ventilated PV cladding. *Solar Energy* **69**, 67-81.
- Candanedo JA, Pogharian S, Athienitis AK & Fry A. (2007). Design and simulation of a net zero energy healthy home in Montreal. *2nd Canadian Solar Buildings Conference* **1**, 1-8.
- Candanedo L, O'Brien W & A.K. A. (2009). Development of an air-based open loop building-integrated photovoltaic/thermal system model. In *Building Simulation 2009*. Glasgow, Scotland
- Charron R. (2004). One- and two-dimensional modelling of ventilated facades with integrated photovoltaics. In *Building, Civil and Environmental Engineering*, pp. 191. Concordia University, Montreal
- Charron R & Athienitis AK. (2006a). Optimization of the performance of double facades with integrated photovoltaic panels and motorized blinds. *Solar Energy* **80**, 482-491.
- Charron R & Athienitis AK. (2006b). A two dimensional model of a double facade with integrated photovoltaic panels. *Journal of Solar Energy Engineering, ASME* **128**, 160-167.
- Chen Y. (2009). Modeling and design of a solar house with focus on a ventilated concrete slab coupled with a building integrated photovoltaic/thermal system. In *BCEE*, pp. 163. Concordia University, Montréal

- 1
2
3 Chen Y, Athienitis AK, Berneche B & Y. P. (2007a). Design and simulation of a building integrated
4 photovoltaic thermal system and thermal storage for a solar home. In *2nd Canadian Solar
5 Buildings Conference*. Calgary
6
- 7 Chen Y, Athienitis AK, Galal KE & Poissant Y. (2007b). Design and Simulation for a Solar House with
8 Building Integrated Photovoltaic-Thermal System and Thermal Storage. In *ISES Solar World
9 Congress, Beijing, China*, pp. 327-332.
10
- 11 Clarke JA, Johnstone C, Kelly N & P.A. S. (1997). The simulation of photovoltaic integrated building
12 facades. *Proc, IBPSA 1997*.
13
- 14 Dittus FW & Boelter LMK. (1930). Heat transfer in automobile radiators of the tubular type. *University of
15 California Publications* **2**, 443-461.
16
- 17 Duffie JA & Beckman WA. (2006). *Solar engineering of thermal processes*. John Wiley & Sons, Inc.,
18 Hoboken.
19
- 20 Eicker U. (2003). *Solar technologies for buildings*. West Sussex.
21
- 22 Eicker U & Fux V. (2000). Heating and cooling potential of combined photovoltaic solar air collector
23 facades. *European Photovoltaic Solar Energy Conference , Glasgow, UK, May 2000*, pp 1836-
24 1839
25
- 26 Fanney AH, Dougherty BP & Davis MW. (2003). Short term characterization of Building Integrated
27 Photovoltaic Panels. *Journal of Solar Energy Engineering, ASME* **125**, 13-20.
28
- 29 Garg HP & Adhikari RS. (1997). Conventional hybrid photovoltaic/thermal (PV/T) air heating collectors:
30 steady-state simulation. *Renewable Energy* **11**, 363-385.
31
- 32 Hegazy AA. (2000). Comparative study of the performance of four photovoltaic/thermal solar air
33 collectors. *Energy Conversion & Management* **41**, 861-881.
34
- 35 Incropera FP & De Witt DP. (2002). *Fundamentals of heat and mass transfer*. John Wiley & Sons.
36
- 37 Ito S, Kashima M & Miura N. (2006). Flow control and unsteady-state analysis on thermal performance of
38 solar air collectors. *Journal of Solar Energy Engineering, ASME* **128**, 354-359.
39
- 40 Ji J, He H, Chow T, Pei G, He W & Liu K. (2009). Distributed dynamic modeling and experimental study
41 of PV evaporator in a PV/T solar-assisted heat pump. *International Journal of heat and mass
42 transfer* **52**, 1365-1373.
43
- 44 King DL, Boyson WE & Kratochvill JA. (2004). Photovoltaic Array Performance Model. Sandia National
45 Laboratories,
46
- 47 King DL, Kratochvil JA & Boyson WE. (1997). Measuring solar spectral and angle-of-Incidence effects on
48 photovoltaic modules and solar irradiance sensors. In *26th IEEE Photovoltaic Specialists
49 Conference*, pp. 5. Anaheim, California
50
- 51 LESO-PB/EPFL L, Enecolo AG M & Ernst Schweizer Ag H. (2000). New generation of hybrid solar pv/t
52 collectors, pp. 55. Swiss Federal Office of Energy,
53
- 54 Liao L. (2005). Numerical and experimental investigation of building-integrated photovoltaic-thermal
55 systems. In *Building, Civil and Environmental Engineering*, pp. 116. Concordia University,
56 Montreal
57
- 58
- 59
- 60

- Liao L, Athienitis AK, Candanedo L, Park K-W, Poissant Y & Collins M. (2007). Numerical and Experimental Study of heat transfer in a BIVP-Thermal system. *Journal of Solar Energy Engineering, ASME* **129**, 423-430.
- Mittelman G, Alshare A & Davidson JH. (2009). A model and heat transfer correlation for rooftop integrated photovoltaics with a passive air cooling channel. *Solar Energy In Press, Corrected Proof.*
- Moshfegh B & Sandberg M. (1996). Investigation of fluid flow and heat transfer in a vertical channel heated from one side by PV elements, part I - Numerical Study. *Renewable Energy* **8**, 248-253.
- Ong KS. (1995). Thermal performance of solar air heaters: mathematical model and solution procedure. *Solar Energy* **55**, 93-109.
- Pantic S. (2007). Energy analysis of photovoltaic thermal system integrated with roof and HVAC system. In *Building, Civil and Environmental Engineering*, pp. 215. Concordia University, Montreal
- Saelens D, Roels S & Hens H. (2004). The inlet temperature as a boundary condition for multiple-skin facade modelling. *Energy and Buildings* **36**, 825-835.
- Sandia National Laboratories. (2006). Database of Photovoltaic Module Performance Parameters.<<http://photovoltaics.sandia.gov/docs/Database.htm>>
- Sharples S & Charlesworth PS. (1998). Full-scale measurements of wind-induced convective heat transfer from a roof-mounted flat plate solar collector. *Solar Energy* **62**, 69-77.
- Sopian K, Yigit KS, Liu HT, Kakac S & Veziroglu TN. (1996). Performance Analysis of photovoltaic thermal air heaters. *Energy Conversion and Management* **37**, 1657-1670.
- Test FL, Lessmann RC & Johary A. (1981). Heat transfer during wind flow over rectangular bodies in the natural environmental. . *Transactions of the ASME J Heat transfer* **103**, 262-267.
- Yang HX, Marshall RH & Brinkworth BJ. (1996). Validated simulation for thermal regulation of photovoltaic structures. *Photovoltaic Specialists Conference, 1996, Conference Record of the Twenty Fifth IEEE.*

1
2
3 Response to Program Administrator,
4

5 Dear Tiffany D. Cox,
6

7 I am attaching the revised version of Manuscript TRNS-0088-2009.R3
8

9 The number of figures has been reduced to 12. Figure 12b containing the
10 pressure drop was removed.
11

12 Please let us know if the new manuscript complies with the
13 requirements. We are looking forward to have it for the 2010 Winter
14 Conference.
15

16 Thank you so much for your time.
17

18 Best regards,
19

20 Luis
21
22
23
24
25
26
27
28
29
30
31
32 11-Sep-2009
33
34 Transactions Paper TRNS-00088-2009.R1 - Transient and Steady State
35 Models for Open-Loop Air-Based BIPV/T Systems
36

37 Dear Luis Candanedo:
38

39 The above manuscript has completed review. Please note that the
40 following editorial requirement has to be met prior to receiving an
41 acceptance letter:
42

43 Please reduce the number of figures to 13. Currently the document has
44 14 figures. Please see author's manual at www.ashrae.org for more
45 details or specifics on figure count.
46

47 Upon receipt of a revised file, I will send to you an acceptance letter
48 for presentation at the 2010 Winter Conference.
49

50 I hope to hear from you soon.
51

52 Best regards,
53

54 Tiffany D. Cox
55 Conference Program Administrator
56
57
58
59
60

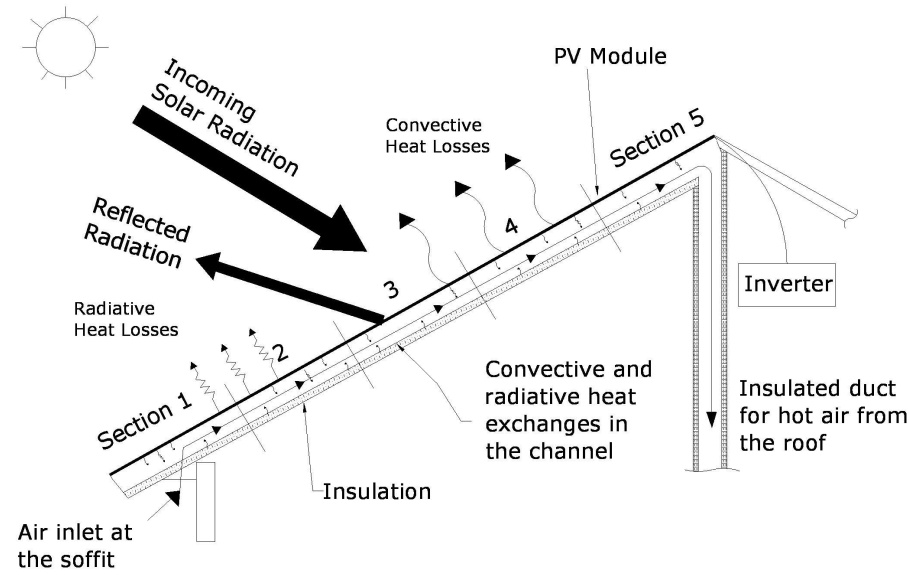
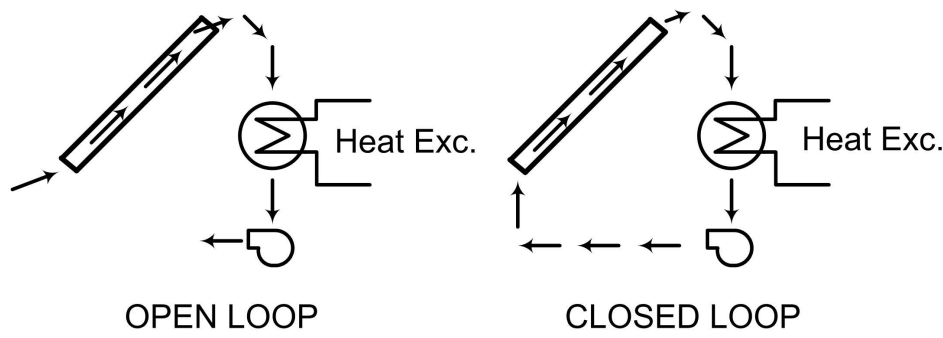
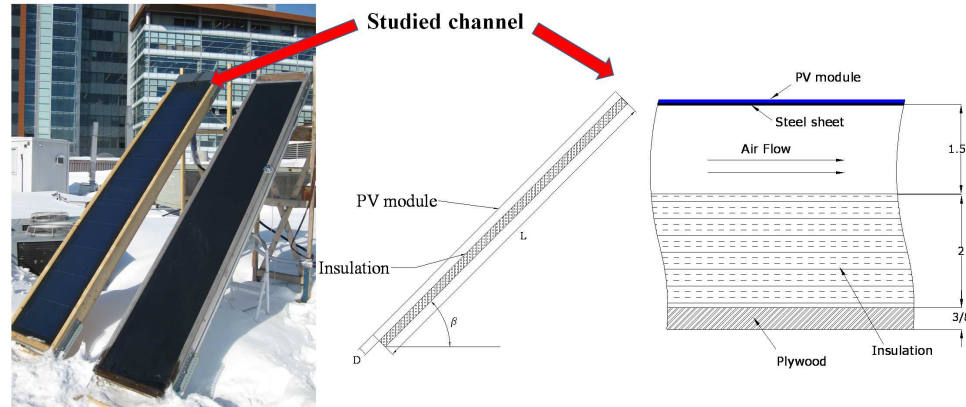


Figure 1. Schematic of a typical air-based open-loop BIPV/T system (Athienitis, 2008)
609x609mm (96 x 96 DPI)



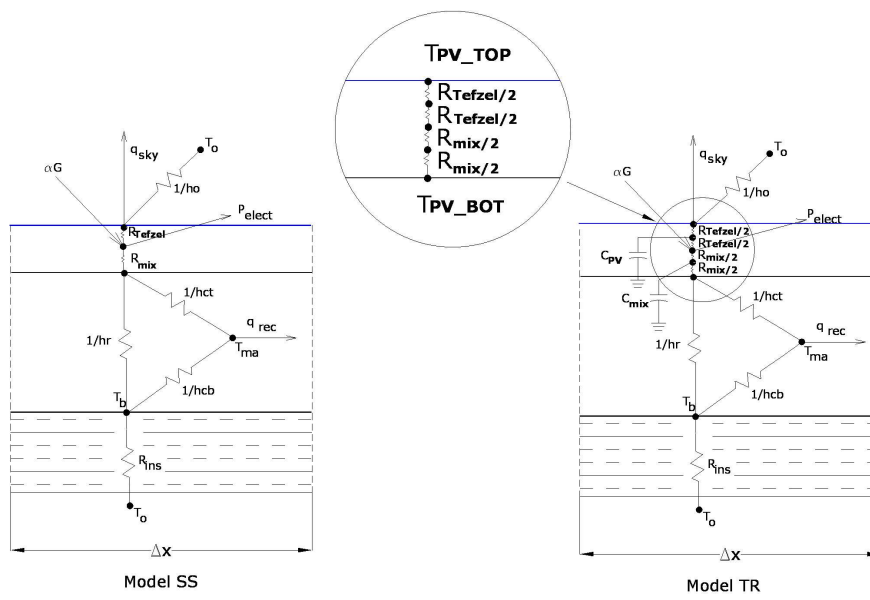


Open and closed loop configurations for solar collectors (the heat exchanger may be eliminated in the open loop configuration).
609x609mm (96 x 96 DPI)

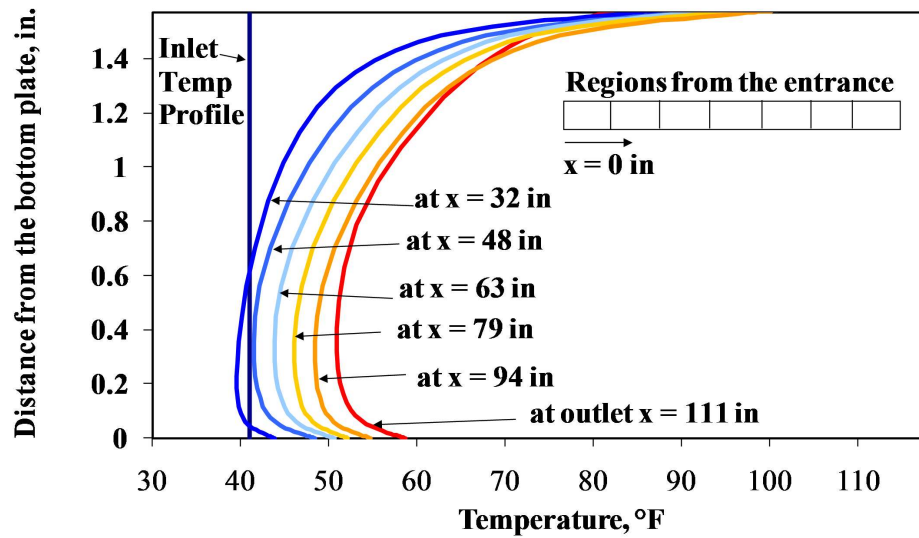


Experimental set-up used for model development. From left to right: photograph of the BIPV/T channel, simplified side view and details of the channel configuration (dimensions in inches).
609x609mm (96 x 96 DPI)

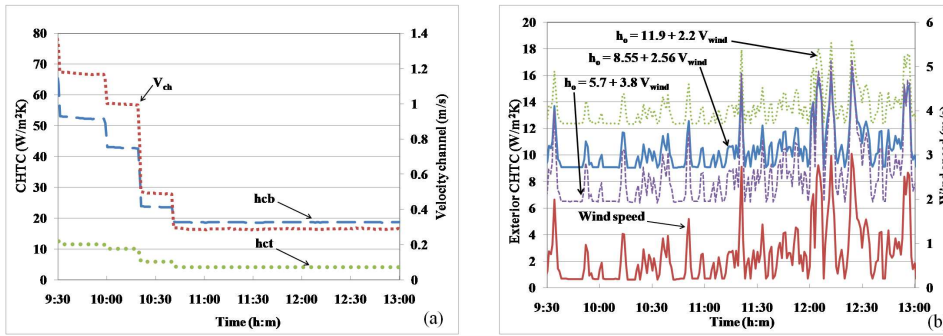
1
2
3
4
5
6
7
8
9
10
11
12
13
14
15
16
17
18
19
20
21
22
23
24
25
26
27
28
29
30
31
32
33
34
35
36
37
38
39
40
41
42
43
44
45
46
47
48
49
50
51
52
53
54
55
56
57
58
59
60



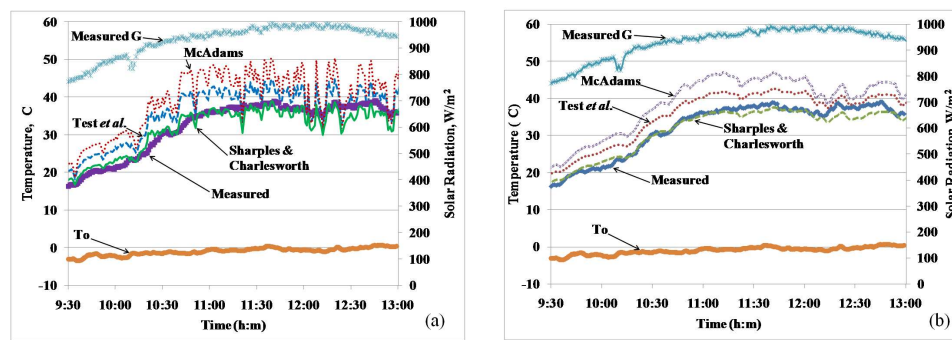
Models studied: Model SS (steady state) and Model TR (transient).
609x609mm (96 x 96 DPI)



Air temperature profiles within the channel as predicted by CFD simulations.
609x609mm (96 x 96 DPI)

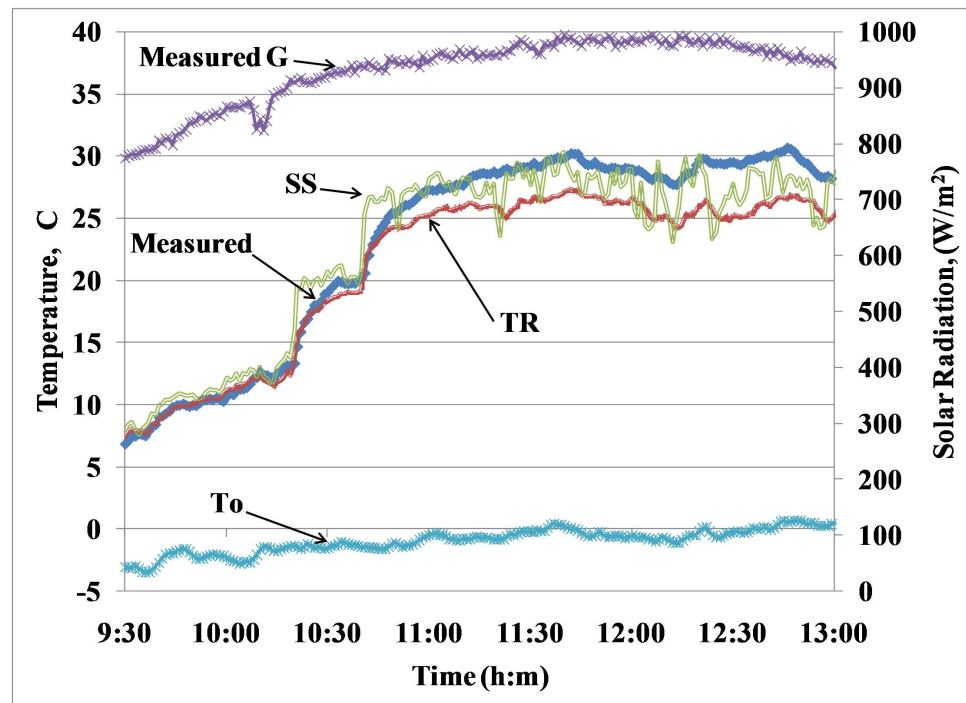


(a) Measured average air speed in the channel, and estimated interior heat transfer coefficients; (b)
Wind speed and exterior heat transfer coefficient.
609x609mm (96 x 96 DPI)



(a) Average temperature of the top of the BIPV/T channel (measurements, Model SS), (b) Average temperature of the top of the BIPV/T channel (measurements, Model TR) Solar radiation incident on collector (G) and exterior air temperatures (To) are also shown.

609x609mm (96 x 96 DPI)



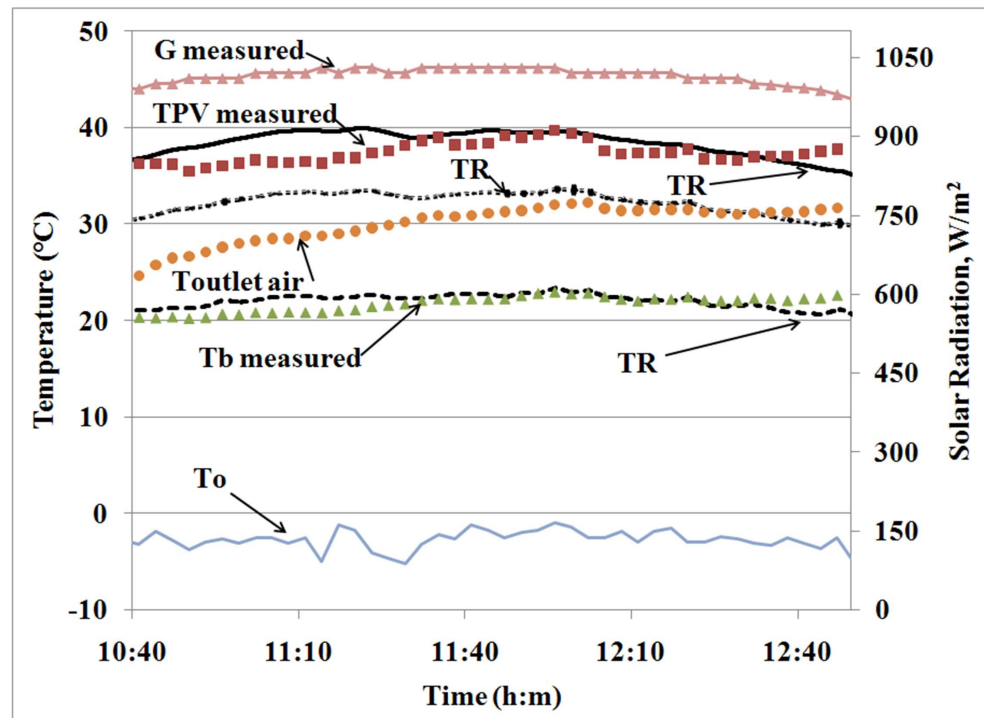
41 Outlet air temperatures (measurements, Model SS and Model TR)
42 609x609mm (96 x 96 DPI)



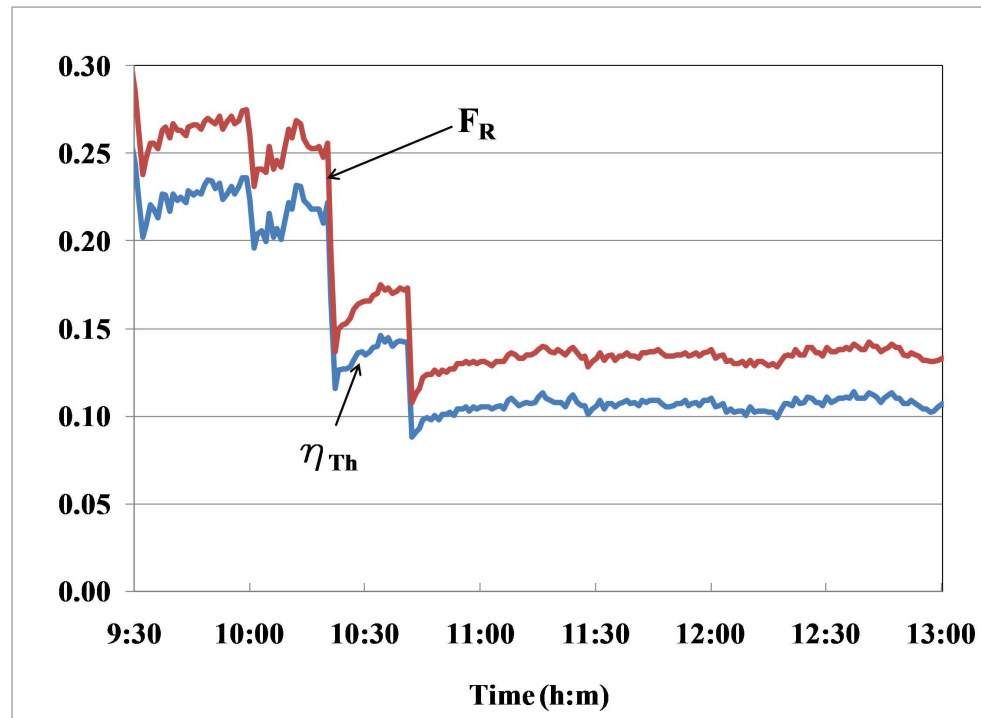
Left: BIPV/T module of the roof under construction in the factory (before installing metal layer and PV modules) Right: BIPV/T module completed (with PV modules installed).
609x609mm (96 x 96 DPI)



EcoTerra™ solar house photograph
609x609mm (96 x 96 DPI)



Temperature profiles for the EcoTerra house on March 17th, 2008 (measurement and Model TR)
609x609mm (96 x 96 DPI)



Heat removal factor and thermal efficiency of the BIPV/T channel.
609x609mm (96 x 96 DPI)